RSC Advances

ROYAL SOCIETY OF CHEMISTRY

www.rsc.org/advances

Synthesis and photochemical properties of BODIPY-functionalized silica nanoparticle for imaging Cu^{2+} in living cells

Xiaoting Yu, Xu Jia, Xiaolong Yang, Weisheng Liu, Wenwu Qin*

Key Laboratory of Nonferrous Metal Chemistry and Resources Utilization of Gansu Province and State Key Laboratory of Applied Organic Chemistry, College of Chemistry and Chemical Engineering, Lanzhou University, Lanzhou 730000, P. R. China.

Abstract A highly selective copper(□) sensor based on BODIPY-functionalized silica nanoparticle, BODIPY-DPA@SN, has been designed and synthesized. Its absorption and fluorescence maxima in dry organic solvents are red-shifted by ~75 and ~50 nm compared to those of BODIPY fluorophore, and are blue-shifted by ~55 and ~15 nm in aqueous-organic (1:1, V/V) media with fluorescence enhancement. The fluorescence intensity almost increases linearly as a function of water concentration (below 5 %, v/v). BODIPY-DPA@SN exhibits high specificity for Cu^{2+} over other transition metal ions in aqueous-organic media, resulting in notable fluorescence quenching and visible pink-to-yellow color change. Confocal microscopy experiment successfully proved that BODIPY-DPA@SN can be a biosensor of copper in living cells.

Introduction

Imaging techniques in living cells are now feasible and effective for the observation of the event on molecular level. Fluorescence is widely applied to monitor the

* To whom correspondence should be addressed. E-mail for W. Qin: qinww@lzu.edu.cn, Tel.: +86-931-8912582; Fax: +86-931-8912582

intracellular consistency of important ions and molecules, and the advances are remarkable.[1,2] Of major importance are fluorophore targeting transition and heavy metal ions (such as Ni^{2+}, Cu^{2+}, Zn^{2+}, Cd^{2+}, Hg^{2+} etc). Considerable amount of fluorescent labeling reagents are organic fluorophores with flexible applications and versatile chemical properties. However, there are still many problems to be solved to target effectively in intracellular level, especially the toxicity of the fluorophore.

4,4-Difluoro-4-bora-3a,4a-diaza-*s*-indacene (BODIPY) **2** [3,4,5] derivatives are fluorescent dyes with noteworthy advantages such as high fluorescence quantum yields, large molar absorption coefficients, high stability towards chemicals and light, and negligible intersystem-crossing.[6] Moreover, BODIPY dyes are excitable with visible light, have narrow emission bandwidths with high peak intensities, and are amenable to structural modification, providing tunable spectral characteristics.

Since paramagnetic Cu^{2+} is a notorious fluorescence quencher, very few ratiometric fluorescent chemosensors for Cu^{2+} are available in the literature.[7] The first fluorescent chemosensor for Cu^{2+} based on BODIPY as a reporter subunit (K_d = 3 μM) was published in 2006.[8] It had 8-hydroxyquinoline as a receptor and showed significant fluorescence quenching in the presence of Cu^{2+} and Hg^{2+} with markedly higher selectivity for Cu^{2+} than Hg^{2+}. A fluorescent off/on BODIPY-based chemosensor which displayed a chelation enhanced fluorescence effect with Cu^{2+} (K_d = 20 μM), Pb^{2+} (K_d = 0.1 mM) and Zn^{2+} (K_d = 2 mM) was described by Yoon et al.[9] Bis(pyridin-2-ylmethyl)amine [commonly known as di(2-picolyl)amine, DPA] is a chelator of several metal ions, including Mn^{2+}, Fe^{2+}, Co^{2+}, Ni^{2+}, Cu^{2+}, Zn^{2+}, Ag^{+}, Cd^{2+}, Hg^{2+} and Pb^{2+}.[10] A colorimetric and NIR fluorescent turn-on BODIPY-based probe with DPA as a chelator

with high selectivity for Cu^{2+} among many transition metal ions has been reported by Boens.[11] Furthermore, many sensors for Cu(□) detection based on nanoparticles with excellent selectivity and efficiency have been developed. Jiang described an optical sensor of copper with upconverting luminescent nanoparticles as an excitation source.[12] An highly luminescent colloidal Eu^{3+}-doped $KZnF^3$ nanoparticle for detection of Cu(□) ions was reported by Mahalingam.[13] Silica nanoparticle is environmentaly friendly non-toxic material with additional properties beneficial for optical imaging applications in biological systems, including chemical inertness, transparency, and the ability to act as stabilizers in protecting the embedded dyes from the outside environment.[14]

In a previous paper, we reported the preparation and spectroscopic properties of BODIPY-DPA (**2**) functionalized hydroxyapatiite (HA) nanoparticles.[15] BODIPY-DPA@THA nanoparticles are not well soluble in aqueous solution due to the low solubility and agglomeration of nano-hydroxyapatiite. Based on the above research results, we developed a turn off probe **1** of copper(□) ions based on BODIPY -functionalized nanoparticles. It had di(2-picolyl)amine (DPA) modified at the 3-position of BODIPY as the ion recognition subunit and silica NP coupled at the 5-position as the hydrophilic matrix to amplify the optical signal and improve the sensitivity. The solvent-dependent photophysical properties and the response to Cu^{2+} ions were investigated.

Experimental section

Materials and methods

Di-(2-picolyl) amine (DPA) and p-tolualdehyde were purchased from HEOWNS Company; trifluoroacetic acid, N-chlorosuccinimide, chloranil, tetraethyl orthosilicate (TEOS) and 3-aminopropyl-triethoxysilane were obtained from TCI Company. Boron

trifluoride diethyl etherate was obtained from Alfa Aesar. The metal ions solutions were prepared from their perchlorate salts. Other materials for the synthesis were acquired from commercials and used without further purification.

Sensor **1** was characterized by transmission electron microscopy (TEM), dynamic scattered light (DSL), thermal gravity analysis (TG) test, UV-vis absorption and fluorescence spectroscopy. Fig. 1a showed the TEM image of SN, with spherical structure of the average size of 200 nm. Fig. 1b revealed the nanocrystalline appearance of **1**. The dynamic light scattering (DLS) analysis at room temperature shows that the average hydrodynamic diameters of **1** is 347 nm (Fig. 1c), which is due to the interaction between the dye **2** functionalized surface and the solvent. The thermal behavior of **1** was studied by thermal gravity analysis (TG) in nitrogen environments (Fig. 1d). A constant mass flow of nitrogen at the rate of 60 mL/min was set for the test. 4.69% of **1** disappeared at around 106 °C, which is due to the very little water. Then **1** began to lose the surface-modified **2** (mp 182-183 °C) at 180 ℃ and totally disappeared 15.71% of it at 535 °C. The loss of 11.02% of the weight is due to the organic dye **2**.

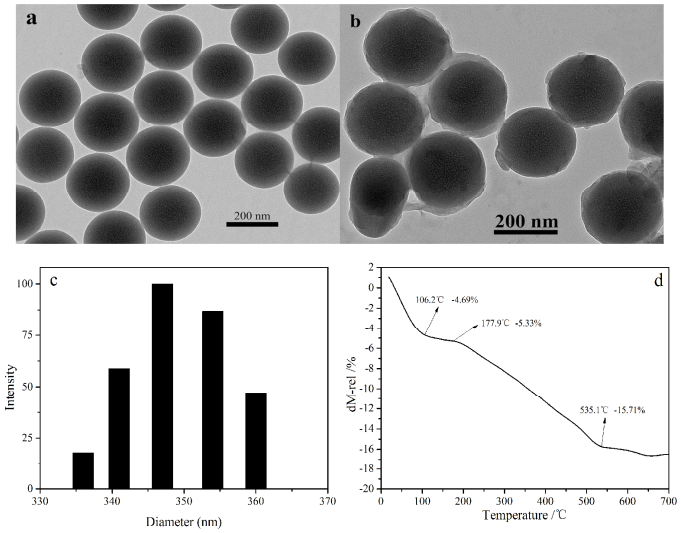

Figure 1 TEM images of (a) silica NPs, (b) **1**, (c) particle size distribution of **1** and (d) TG curve of **1**.

In the infrared spectrum (Fig. S1) of SN, Si-O main bands are at 1098 (υ_{as}) cm^{-1}, 800 (υ_s) and 956 (δ) cm^{-1}, hydroxide bands at 3431 (υ_s) and 1633 (δ) cm^{-1}. The amino and $-CH_2-$ groups also give 1570 (δ) cm^{-1} and 2922 (υ_s) cm^{-1}. In the IR spectrum of **1**, new strong bands at 2965, 2852, 1869 and 1535 cm^{-1} appear in accordance with **2** bonding covalently to the SN nanoparticles.

Apparatus

^1H and ^{13}C NMR spectra were taken on a Bruker DRX-400 spectrometer with TMS as an internal standard and $CDCl_3$ as solvent. Mass spectra were recorded in E.I. mode. Melting points were measured on an X-4 micro-melting point apparatus (Gongyi Yuhua Instrument Co.).The transmission electron microscopy images (TEM) were obtained on a JEM-2100 transmission electron microscope at an acceleration voltage of 120 kV. The hydrodynamic diameter and size distribution was measured with dynamic scattered light (BI-200SM) at room temperature using ethanol/water as the solvent. The thermal gravity analysis (TG) test was measured by STA PT1600 instrument of Linseis Company of

Germany. UV–vis absorption spectra were recorded on a Varian UV-Cary100 spectrophotometer and for the corrected steady-state excitation and emission spectra, a Hitachi F-4500 and a FLS920 spectrofluorometers were employed. For the determination of fluorescence quantum yields ϕ_f of **1** and **2**, only dilute solutions with the absorbance below 0.1 at the excitation wavelength (λ_{ex} = 480 or 500 nm) were used. Rhodamine 6G in water (ϕ_f = 0.92) and rhodamine B in water (ϕ_f = 0.31) were used as fluorescence standard.[16] Fluorescence decay histograms were obtained on an Edinburgh instrument FLS920 spectrometer equipped with a supercontinue white laser (400-700 nm), using the time-correlated single photon counting technique in 2048 channels. Histograms of the instrument response functions (using a LUDOX scatterer) and sample decays were recorded until they typically reached 5×10^3 counts in the peak channel.

Synthesis of BODIPY-DPA The compound **2** was synthesized according to a literature procedure,[17] Orange powder. Yield: 72%; mp 182-183 °C. ^{1}H NMR ($CDCl_3$, 400 MHz): δ = 2.42 (s, 3H, tolyl-CH_3), 5.24 (s, 4H,-CH_2-), 6.21 (d, 1H, *J* = 4.0 Hz, H-2), 6.28 (d, 1H, *J* = 4.8 Hz, H-1), 6.33 (d, 1H, *J* = 4.0 Hz, H-7), 6.81 (d, 1H, *J* = 5.2 Hz, H-6), 7.19 (dd, 2H, *J* = 5.2 Hz, *J* = 2.0 Hz, 2H, H-5'), 7.24 (d, 2H, *J* = 8.0 Hz, H-3'), 7.33 (d, 2H, *J* = 8.0 Hz, aromatic), 7.41 (d, 2H, *J* = 8.0 Hz, aromatic), 7.67 (td, 2H, *J* = 7.6 Hz, *J* = 1.6 Hz, H-4'), 8.55 (d, 2H, *J* = 4.8 Hz, H-6'); ^{13}C NMR ($CDCl_3$, 100 MHz): δ 21.28, 57.93, 113.18, 115.02, 119.61, 122.00, 122.63, 128.82, 130.22, 130.36, 131.29, 132.48, 135.13, 135.43, 137.02, 139.22, 149.37, 156.23, 163.87; IR (KBr) ν_{max}/cm^{-1} 995-700(m), 1059(s), 1111(s), 1158(m), 1261(m), 1305(m), 1416(s), 1435(s), 1535(m), 1585(s), 1627(s), 1869(m), 2852(m), 2924(m), 2965(m), 3437(s); MS (ESI) *m/z* calcd. For $C_{28}H_{23}BClF_2N_5$ 513.2; found 514.3(M+1, 100%).

Synthesis of BODIPY-DPA@SN The synthetic route is depicted in Scheme 1. APTES modified silica nanoparticles (1.0 g) were dispersed in 30 mL of acetonitrile by ultrasonication, 1.0 mL of triethylamine was added, and the mixture was stirred for 30 min, 30 mL of BODIPY-DPA (500 mg) acetonitrile solution was injected into the mixture, and the reaction mixture was stirred and refluxed for 12 h in the dark. Then washed and dispersed with DI water and ethanol for several times. BODIPY-DPA@SN was obtained by centrifuge and dried overnight, followed by dialysis for 5 days to remove the free dyes.

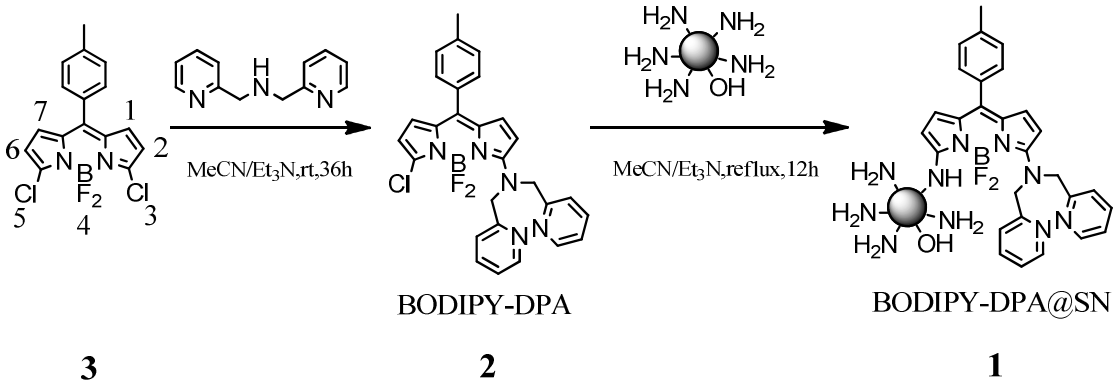

Scheme 1 Synthesis of BODIPY-DPA@SN (**1**).

Binding copper The titration experiments with copper were carried out by adding small quantities of stock ethanol-water (1:1, V/V) solution of metal perchlorate salts to a larger volume (25 mL) of solution of **1**. The ground-state dissociation constants K_d of the BODIPY-DPA@SN-Cu complex was determined in ethanol-water solution (1:1, V/V) by fluorometric titration. Nonlinear fitting of eqn. (1) [18] to the steady-state fluorescence data F recorded as a function of [Cu^{2+}] yields values of K_d. The fluorescence signals F_{min} and F_{max} at minimal and maximal [Cu^{2+}] respectively correspond to the free and Cu^{2+} bound forms of the nano-probe, and n stands for the number of copper ions bound per probe.

$$F = \frac{F_{max}\left[Cu^{2+}\right]^n + F_{min}K_d}{K_d + \left[Cu^{2+}\right]^n} \quad (1)$$

Fluorescence decay Fluorescence lifetime was measured by a FLSP920 spectrofluorometer at room temperature. **1** was dissolved in aqueous-organic media (1:1, V/V) and the concentration was adjusted to make the optical densities <0.1 at the excitation wavelength. The monitored wavelengths were 580 nm, 590 nm and 600 nm, and the excitation wavelength was 480 nm.

Cell culture The SMMC-7721 cells were provided by the Institute of Biology (Lanzhou University). To determine the cell permeability of **1**, the cells were incubated with 1 mg/L of **1** (0.1% ethanol) for 30 min at 37 °C, and washed with 4-(2-Hydroxyethyl)-1-piperazineethanesulfonic acid (HEPES) to remove the remaining **1**. To observe the fluorescence changes of the medium, 0.5 μM of Cu^{2+} were added into the **1**-loaded cells to preincubated for 0.5 h at 37 °C, followed by further incubation with 0.1 mM Na_2S for 0.5 h. The confocal fluorescence imaging was performed with a Leica DM-4000D microscope.

Results and discussion

The absorption spectra of **2** is similar of BODIPY dyes,[19,20,21,22,23,24] with an intense absorption band that maximum λ_{abs} located at 505 nm, assigned to the 0–0 band of the $S_1 \leftarrow S_0$ transition, and a shoulder peak (480 nm) on the high-energy side, attributed to the 0–1 vibrational band of the same transition. In addition, a weaker broad absorption band attributed to the $S_2 \leftarrow S_0$ transition is found around 350 nm. The maximum emission wavelength λ_{em} is 556 nm. The absorption of **1** show well-known pattern of BODIPY derivatives and the λ_{abs} is red 75 nm-shifted compared to **2** (from 505 to 580 nm) in

ethanol. The fluorescence spectra of **1** display narrow, slightly Stokes-shifted emission band at 605 nm and is 50 nm red-shifted compared to **2** (Fig. 2). The silica NPs show neither absorption nor fluorescence under same conditions (Fig. S2), which demonstrates that there is no energy transfer between silica NPs and BODIPY-DPA dye but the *N*-substitutents at 3- and 5-positions that make contribution to the special spectroscopic change between **1** and **2**.

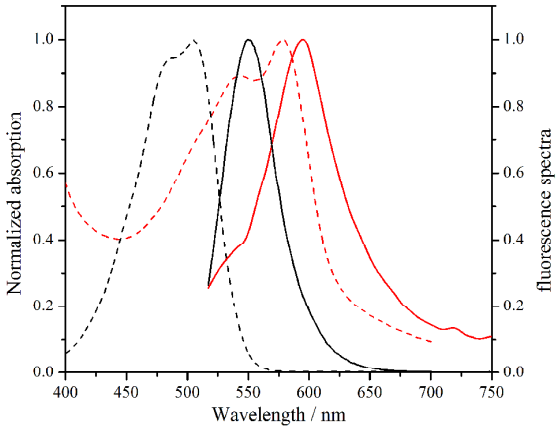

Figure 2 Normalized absorption (dash curves) and fluorescence spectra (solid curves) of **1** (red) and **2** (black). Measured in absolute ethanol and the excitation wavelength λ_{ex} = 500 nm.

Compared to classic BODIPY derivatives, nonsymmetrically substituted (mono-substituted) BODIPY derivatives with an *N*-substitutent at 3-position have wider absorption and emission bands, red-shifted λ_{em}(max) and larger Stokes shifts than symmetric BODIPY dyes.[25] Moreover, there is a large difference in photophysical properties between the mono- and bis-substituted (symmetrically substituted) aminophenyl BODIPY derivatives. The emission wavelength λ_{em}(max) of bis-substituted is shifted further to the red in comparison to the nonsymmetrically substituted.[26] The

differences above suggest the spectroscopic properties of these BODIPY derivatives are mainly effected by the aminophenyl group at the 3- (and 5-) position(s).[27]

Water has been the most widely used solvent for the proton transfer studies due to its proton accepting and conducting properties and recognized as an active participant, rather than just a passive medium in the initial deprotonation step and in the transport mechanism of the proton.[28,29] The effects of water on the emission spectra of two cupreidine derivatives in methanol–water mixed solutions were already reported by Brouwer et al, complexation with water leads to enhanced excited state proton transfer (ESPT) and a fully solvated ‘‘free’’ ion pair (FIP) model can explain this change. [30]With the increase of water content in various solvents, compounds show fluorescence enhancement by suppression of ICT due to the formation of fluorescent ionic structures by hydrolysis[31] (Scheme 2).

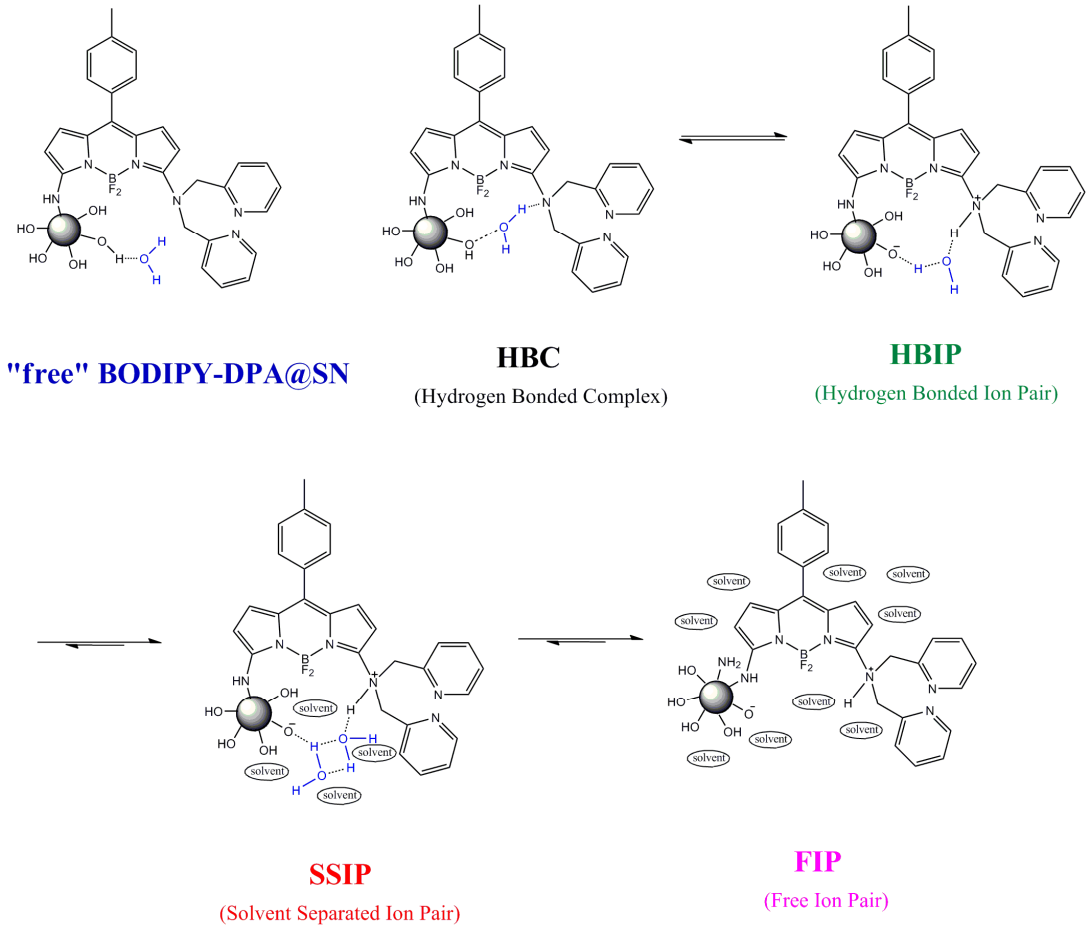

Scheme 2 Simplified reaction scheme of the excited-state free ion pair formation of **1** in ethanol/water media.

Fig. 3 shows the normalized absorption and fluorescence spectra of **1** in aqueous-organic media (1:1, V/V). The maximum λ_{abs} is blue-shifted from 580 to 528 nm and the maximum λ_{em} is also blue-shifted from 610 nm to 590 nm accompanied by a large intensity enhancement.

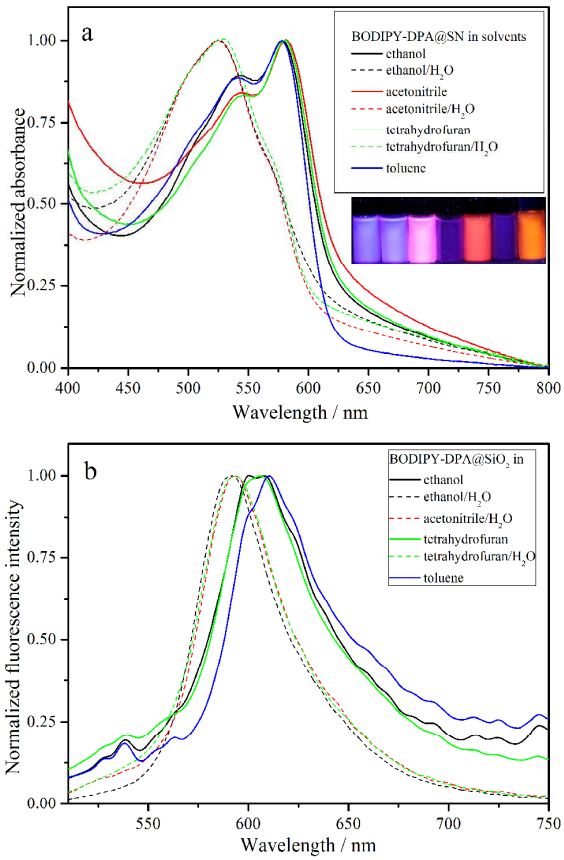

Figure 3 Normalized (a) absorbance and (b) fluorescence spectra of **1** in different solvents. The excitation wavelength λ_{ex} = 480 nm and the vial shows the sensor **1** in different solvents under UV light (left to right: 1. toluene; 2.ethanol; 3.ethanol-water; 4.THF; 5.THF-watere; 6.MeCN; 7.MeCN-water).

Absorption (Fig. S3) and fluorescence spectra of **1** (Fig. 4, keeping the concentration of **1** constant) were measured in ethanol that contained various concentrations of water. Further sonication for 30 min was applied to obtain homodispersed solutions. The main absorption band at 580 nm is blue-shifted and decreased, whereas the band at 525 nm becomes more outspoken, revealing the ground state hydrogen bonding interactions. The fluorescence band maximum is slightly blue-shifted and accompanied by an increase in intensity. The intensity increases almost linearly with the water content lower than 5 %

(V/V) (Fig. S4). However, the fluorescence level off and is no longer dependent on the water content that higher than 25 % (V/V) (Fig. S5).

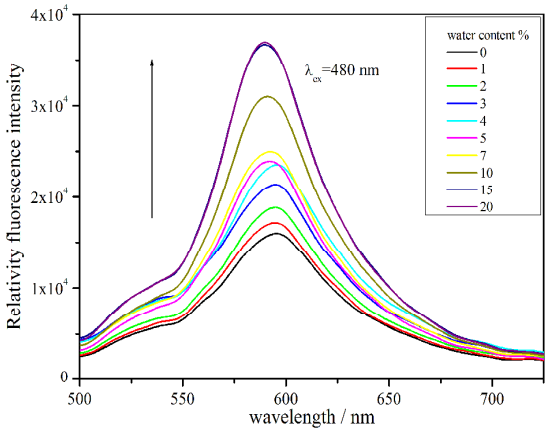

Figure 4 Fluorescence spectra of **1** with different water content in ethanol solution. The excitation wavelength λ_{ex} = 480 nm.

Both the hydroxyl groups that reside on SN surface and the DPA moieties have a high affinity via hydrogen bonding interactions with water, especially in solvents with moderate polarity. The fluorescence spectra of **2** (with same DPA group) exhibited no change with the increasing water content in solvents. Therefore, the results indicate that the fluorescence enhancement of **1** in anhydrous ethanol may be attributed to the suppression of ICT by the hydrogen bonding between the hydroxyl group of ethanol and the tertiary amino group of **1**, and the interaction between the hydroxyl groups that reside on SN, water and the tertiary amino group.[32]

To examine the chelating ability of **1**, UV–vis spectrophotometric and fluorometric titrations were carried out in ethanol-water media (1:1, V/V). Upon addition of Cu^{2+}, the absorption band of **1** exhibited a hypsochromic shift from 525 nm to 455 nm (Fig. S6), and the fluorescence was strongly quenched: Φ_f of **1**–Cu complex is only 0.02 versus 0.14 of **1**. The average K_d value of the **1**–Cu complex amounted to 3.30 ± 0.4 μM (Fig.

5). The adding of Mn^{2+}, Fe^{3+}, Co^{2+}, Ni^{2+}, Zn^{2+}, Ag^{+}, Cd^{2+}, Hg^{2+} and Pb^{2+} to the ethanol/water (1:1, V/V) solutions of **1** caused no changes that could be detected in the UV–vis absorption and fluorescence spectra (Fig. S7), which indicated that the detection of Cu^{2+} is hardly affected by these common coexistent metal ions.

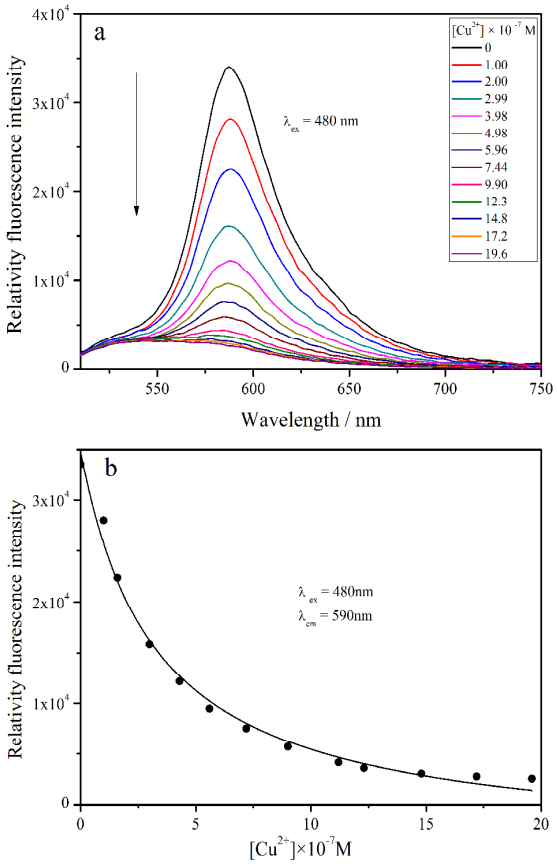

Figure 5 (a) Fluorescence spectra of **1** as a function of $[Cu^{2+}]$ in ethanol/water (1/1, V/V) solution and (b) the best fit to the direct fluorimetric titration data. The concentration of **1** is 50 mg/L, λ_{ex} = 480 nm, λ_{em} = 590 nm.

A near-linear correlation between the fluorescence intensity and Cu^{2+} concentration (r = 0.993, n= 6) was obtained over the range of 0.05–0.72 μM Cu^{2+} (Fig. S8). The

detection limit was 0.1 nM through the calculation by multiplying the standard derivation of 10 blank measurements by 3, and dividing by the slope of the linear calibration of sensor between fluorescence intensity at 590 nm and copper ion concentration in 1:1 ethanol-water (V/V, pH 7.2) solution. This demonstrates the potential utility of the sensor **1** for determination of the copper ion concentration in aqueous solutions.

To verify that if the conuter anion corresponding to Cu^{2+} cation affected the detection, we performed the detection experiments with copper(□) chloride dehydrate and copper(□) nitrate trihydrate as Cu^{2+} sources. The results were very analogous (Fig. S9) and provided the evidence that conter anions have little influence on the dectection of Cu^{2+} ions. So we used copper(Ⅱ) perchlorate in following experiments.

To examine the reversibility of the processes, an excess amount of Na_2S was added to the **1**–Cu complex solution. The fluorescence spectra of **1** as a function of Na_2S concentration are shown in Fig. 6. Upon addition of Na_2S, the S^{2-} reacted with Cu^{2+} to form precipitates and the bright pink fluorescence of **1** immediately turned on. Then we continued to add Cu^{2+} for induced quenching and Na_2S for recovery. After four cycles the fluorescence remained very weak and no longer changed with plenty of Na_2S (Fig. S10). This result clearly implies that probe **1** binds reversibly with Cu^{2+}.

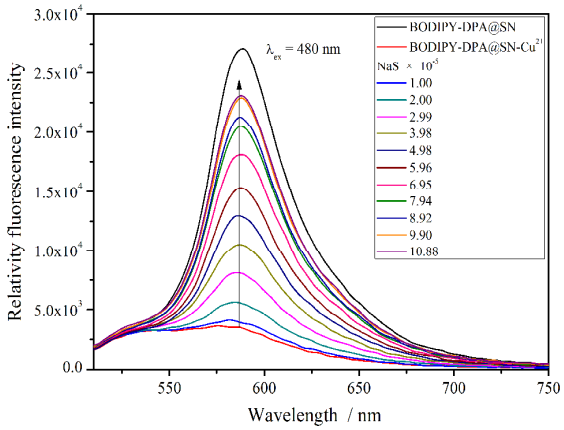

Figure 6 Fluorescence spectra of **1**–Cu complex as a function of [Na_2S]. Measured in ethanol/water (1/1, V/V) solution, λ_{ex} = 480 nm.

For further biological application of copper (Ⅱ) detection, ethanol/water (1/1, V/V) solutions of **1** with different pH (3-10) were applied to confirm the perfect testing environment (Fig. 7). The detection of copper (Ⅱ) ions is most sensitive in neutral solution, which is due to the suppression of complex formation by acid environment and Cu^{2+} sedimentation induced by base environment. We tested the practical applicability of **1** for Cu^{2+}detection in neutral biological environment.

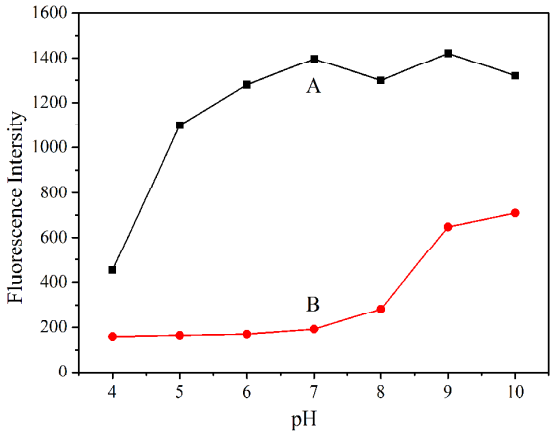

Figure 7 Fluorescence intensity of **1**-Cu in the absence (A) and presence (B) of Cu^{2+} at different pH values. λ_{ex} = 480 nm.

SMMC-7721 cells incubated with **1** initially displayed a strong fluorescence image (Fig. 8a), but the image became black in the presence of Cu^{2+} (Fig. 8c). However, after incubation with sulfide, the fluorescence gradually recovered (Fig. 8e). The experiment clearly demonstrated that **1** is membrane-permeable and the fluorescence changes are due to the synchronous presence of **1** and Cu^{2+}. Herein we believe that **1** can be used to image intracellular Cu^{2+} in living cells.

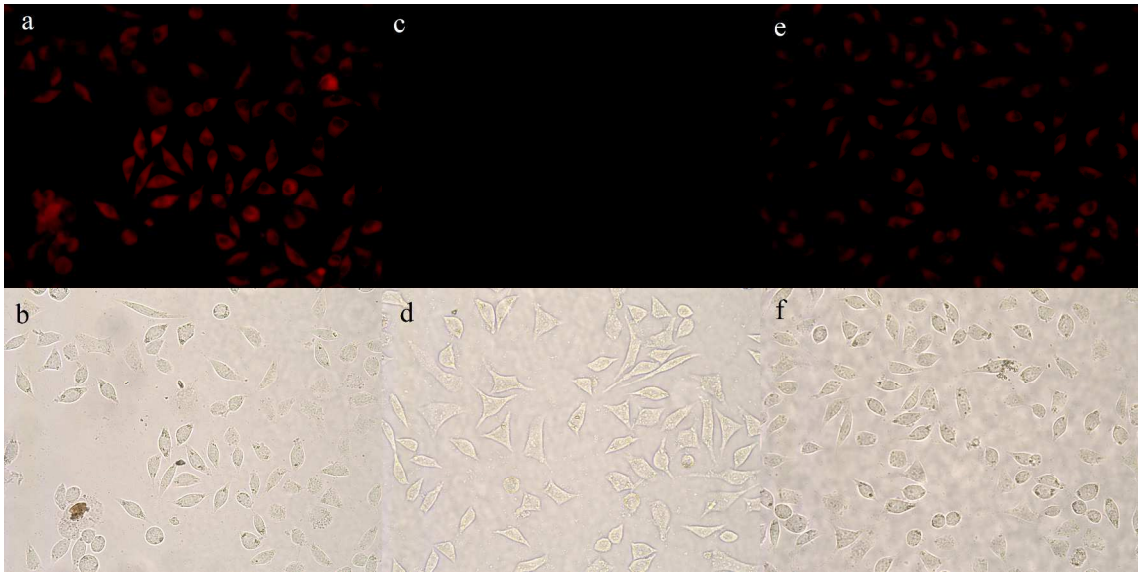

Figure 8 Confocal fluorescence images of SMMC-7721 cells in red (570–620 nm) emission channel. (a) Fluorescence image and (b) bright field microscopy image of cells incubated with 1 mg/L of **1** (0.1% ethanol) for 30 min; (c) Fluorescence image and (d) bright field microscopy image of **1**-stained cells exposed to 0.5 μM of Cu^{2+} for 30 min. (e) Fluorescence image and (f) bright field microscopy image of cells preincubation with **1** and Cu^{2+} followed by incubation with Na_2S for 30 min.

To investigate the fluorescence dynamics of **1**, fluorescence decay traces in different aqueous-organic (water-ethanol, water-THF and water-MeCN) media (1:1, V/V) were collected as a function of emission wavelength λ_{ex} (Fig. 9). The fluorescence lifetimes of

1 in pure solvents were too short and could not be determined. The results of the time-resolved fluorescence experiments are shown in Table 1 and Fig. S9.

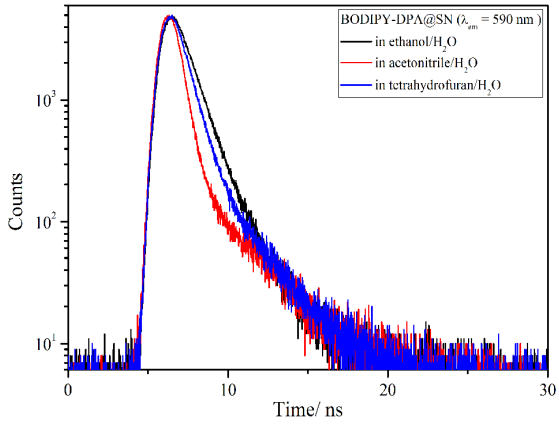

Figure 9 Fluorescence decay curves of **1** in different aqueous-organic media.

Table1 Photophysical data of **1**, **2** and **1**-Cu complex

Complex	Solvent	λ_{abs}(max) / nm	λ_{em}(max) / nm	Φ_f
	cyclohexane	518	555	0.009
	toluene	516	557	0.009
2	THF	503	554	0.006
	EtOH	506	551	0.008
	MeCN	485	553	0.005
	toluene	579	610	0.006
	THF	580	605	0.004
	EtOH	580	605	0.004
1	MeCN	580	605	<0.0005
	THF/H_2O(1:1)	528	593	0.10
	EtOH/H_2O(1:1)	525	592	0.14
	MeCN/H_2O(1:1)	525	593	0.05
1–Cu	EtOH/H_2O(1:1)	455	592	0.02

The fluorescence decay of **1** in ethanol/water (1:1, V/V) solution in the region of 580-600 nm was fitted to the bi- exponential profile with the decay times of 4.50 ns (3%) and 1.05 ns (97%). Fluorescence decay of **1** in THF-water solution (1:1, V/V) and MeCN-water solution (1:1, V/V) also revealed bi-exponential behavior, but the decays become

shorter (Table S1). Most probably, there is equilibrium between monomers and aggregates in the ground state. The slow decay might be attributed to the lifetime of aggregates while the fast decay may be attributed to the deactivation of the monomer molecules.

The complex formation between **1** and Cu^{2+} was also investigated by time-resolved fluorescence. Upon addition of Cu^{2+} to **1**, the longer decay time decreases (~4.50 to ~3.50 ns) along with an increase in the amplitude (~3% to ~25%). The shorter component remains constant (~1.05 ns), and in general, the contribution from this component decreases (~97% to ~75%) (Table S1)**.**

Conclusions

A BODIPY based fluorescent chemosensor **1** was synthesized by a nucleophilic substitution of BODIPY derivative with silica nanoparticles. Unlike literature values for BODIPY–Fe_3O_4, Ni or gold nanoparticles and their corresponding BODIPY sensors, there is quite a large difference in the properties between the free BODIPY-DPA dye and the BODIPY-DPA@SN. The absorption and fluorescence maxima of **1** in organic-water media are blue-shifted compared to in dry solvents, and red-shifted compared to BOPIDY-DPA. The fluorescence intensity was greatly enhanced after the addition of water to organic solvents (polar, less polar, protic and aprotic solvents) and sonication, which is attributed to the suppression of ICT by the formation of the FIP structure**. 1** formed 1:1 complex with Cu^{2+} in ethanol/water (1/1, V/V) solution that resulted in the distinct fluorescence decease that can be observed by naked eye. When Na_2S solution is added to the complex, copper ions were released and the fluorescence recovered. The fluorescence decay of **1** in aqueous-organic media (1:1, V/V) in the region of 580-600 nm

is fitted to the bi- exponential profile. Confocal microscopy experiment shows the potential utilization of chemosensor **1** for fluorescent imaging of Cu^{2+} levels in living cells.

Acknowledgement

This work was supported by the Chinese "Program for New Century Excellent Talents in University" (NCET-09-0444), the "Fundamental Research Funds for the Central Universities" (lzujbky-2011-22 and lzujbky-2012-k13), the National Science Foundation for Fostering Talents in Basic Research of the National Natural Science Foundation of China (Grant No. J1103307) and the "International Cooperation Program of Gansu Province" (1104WCGA182). The authors would like to thank the Natural Science Foundation of China (No. 21271094), and this study was supported in part by the "Key Program of National Natural Science Foundation of China" (20931003).

Electronic Supplementary Information (ESI) Available:

Compound characterization data, absorption and fluorescence spectra can be found in the Supporting Information.

References

1 J. P. Desvergne, A. W. Czarnik, in *Chemosensors of Ion and Molecule Recognition*, (Eds: Kluwer: Dordrecht), the Netherlands, 1997.

2 B. Valeur, J. C. Brochon, in *New Trends in Fluorescence Spectroscopy Applications to Chemical and Life Sciences*, Springer, Berlin, 2002.

3 A. Treibs, F. H. Kreuzer, *Liebigs Ann. Chem.*, 1968, **718**, 208.

4 (a) A. Loudet, K. Burgess, *Chem. Rev.*, 2007, **107**, 4891; (b) G. Ulrich, R. Ziessel, A. Harriman, *Angew. Chem. Int. Ed.*, 2008, **47**, 1184.

5 R. P. Haugland, The Handbook. *A Guide to Fluorescent Probes and Labeling Technologies,* 10th ed., Invitrogen–Molecular Probes, Carlsbad, CA, 2005.

6 The following represents a non-exhaustive list of BODIPY papers with spectroscopic/ photophysical data. (a) E. V. Wael, J. A. Pardoen, J. A. Koeveringe, J. Lugtenburg, *Recl. Trav. Chim. Pays-Bas,* 1977, **96**, 306; (b) J. Karolin, L. B. Johansson, L. Strandberg, T. Ny, *J. Am. Chem. Soc.*, 1994, **116**, 7801; (c) M. Kollmannsberger, K. Rurack, U. Resch-Genger, J. Daub, *J. Phys. Chem. A*, 1998, **102**, 10211; (d) M. Kollmannsberger, K. Rurack, U. Resch-Genger, W. Rettig, J. Daub, *Chem. Phys. Lett.*, 2000, **329**,363; (e) F. López Arbeloa, J. Bañuelos Prieto, V. Martínez Martínez, T. Arbeloa López, I. López Arbeloa, ChemPhysChem, 2004, **5**, 1762; (f) J. Bañuelos Prieto, F. López Arbeloa, V. Martínez Martínez, T. Arbeloa López, F. Amat-Guerri, M. Liras, I. López Arbeloa, *Chem. Phys. Lett.*, 2004, **385**, 29; (g) M. Baruah, W. Qin, N. Basari, W. M. De Borggraeve, N. Boens, *J. Org. Chem.*, 2005, **70**, 4152; (h) W. Qin, M. Baruah, M. Van der Auweraer, F. C. Schryver, N. Boens, *J. Phys. Chem. A*, 2005, **109**, 7371; (i) W. Qin, M. Baruah, A. Stefan, M. Van der Auweraer, N. Boens, *ChemPhysChem*, 2005, **6**, 2343; (j) Z. Dost, S. Atilgan, E. U. Akkaya, *Tetrahedron*, 2006, **62**, 8484; (k) W. Qin, T. Rohand, M. Baruah, A. Stefan, M. Van der Auweraer, W. Dehaen, N. Boens, *Chem. Phys. Lett.*, 2006, **420**, 562; (l) Z. Li, R. Bittman, *J. Org. Chem.*, 2007, **72**, 8376; (m) W. Qin, T. Rohand, W. Dehaen, J. N. Clifford, K. Driessen, D. Beljonne, B. Van Averbeke, M. Van der Auweraer, N. Boens, *J. Phys. Chem. A*, 2007, **111**, 8588; (n) T. Rohand, J. Lycoops, S. Smout, E. Braeken, M. Sliwa, M. Van der Auweraer, W. Dehaen, W. M. De Borggraeve, N. Boens, *Photochem. Photobiol. Sci.*, 2007, **6**, 1061; (o) Z. Ekmekci, M. D.Yilmaz, E. U. Akkaya, *Org. Lett.*, 2008, **10**, 461; (p) L. Li, J. Han, B. Nguyen, K. Burgess, *J. Org. Chem.*, 2008, **73**,1963.

7 (a) K. A. Mitchell, R. G. Brown, D. Yuan, S. C. Chang, R. E. Utecht, D. E. Lewis, *J. Photochem. Photobiol A: Chem*., 1998, **115**, 157; (b) Z. Xu, Y. Xiao, X. Qian, J. Cui, D. Cui, *Org. Lett.*, 2005, **7**, 889; (c) Z. Xu, X. Qian, J. Cui, *Org. Lett*., 2005, **7**, 3029; (d) H. Yang, Z. Liu, Z. Zhou, E. Shi, F. Li, Y. Du, T. Yi, C. Huang, *Tetrahedron Lett*., 2006, **47**, 2911.

8 Y. Mei, P. A. Bentley, W. Wang, *Tetrahedron Lett*., 2006, **47**, 2447.

9 X. Qi, E. J. Jun, L. Xu, S. J. Kim, J. S. J. Hong, Y. J. Yoon, *J. Org. Chem*., 2006, **71**, 2881.

10 K. Kiyose, H. Kojima, Y. Urano, T. Nagano, *J. Am. Chem. Soc.*, 2006, **128**, 6548.

11 S. Yin, V. Leen, S. Van Snick, N. Boens, W. Dehaen, *Chem. Commun*., 2010, **46**, 6329.

12 J. Zhang, B. Li, L. Zhang, H. Jiang, *Chem. Commun*., 2012, **48**, 4860.

13 S. Sarkar, M. Chatti, V. Mahalingam, *Chem. Euro. J*., 2014, **20**, 3311.

14 R. P. Bagwe, X. Zhao, W. Tan, *J. Dispers. Sci. Technol*., 2003, **3&4**, 453.

15 X. Jia, X. Yu, G. Zhang, W. Liu, W. Qin, *J. Coord. Chem.*, 2013, **66**, 662.

16 J. Olmsted, *J. Phys. Chem.*, 1979, **83**, 2581.

17 B. J. Litter, M. A. Miller, C. H. Hung, R. W. Wagner, D. F. O'Shea, P. D. Boyle, J. S. Lindsey, *J. Org. Chem.*, 1999, **64**, 1391.

18 E. Cielen, A. Tahri, K. Ver Heyen, G. J. Hoornaert, F. C. De Schryver, N. Boens, *J. Chem. Soc.*, 1998, **2**, 1573.

19 K. Rurack, M. Kollmannsberger, J. Daub, *Angew. Chem. Int. Ed.*, 2001, **40**, 385.

20 K. Rurack, M. Kollmannsberger, J. Daub, *New. J. Chem.*, 2001, **25**, 289.

21 A. Coskun, E. U. Akkaya, *J. Am. Chem. Soc.*, 2005, **127**, 10464.

22 M. Baruah, W. Qin, C. Flors, J. Hofkens, R. A. L. Vallée, D. Beljonne, M. Van der Auweraer, W. M. De Borggraeve, N. Boens, *J. Chem. Phys. A,* 2006, **110**, 5998.

23 T. López Arbeloa, F. López Arbeloa, I. López Arbeloa, I. García-Moreno, A. Costela, R. Sastre, F. Amat-Guerri, *Chem. Phys. Lett.*, 1999, **299**, 315.

24 A. Costela, I. García-Moreno, C. Gomez, R. Sastre, F. Amat-Guerri, M. Liras, F. López Arbeloa, J. Bañuelos Prieto, I. López Arbeloa, *J. Phys. Chem. A*, 2002, **106**, 7736.

25 W. Qin, V. Leen, T. Rohand, W. Dehaen, P. Dedecker, M. Van der Auweraer, K. Robeyns, L. Van Meervelt, D. Beljonne, B. Van Averbeke, N. Clifford, K. Driesen, K. Binnemans, N. Boens, *J. Phys. Chem. A*, 2009, **113**, 439.

26 W. Qin, V. Leen, W. Dehaen, J. Cui, C. Xu, X. Tang, W. Liu, T. Rohand, D. Beljonne, B. Van Averbeke, J. N. Clifford, K. Driesen, K. Binnemans, M. Van der Auweraer, N. Boens, *J. Phys. Chem. C*, 2009, **113**, 11731.

27 X. Jia, X. Yu, X. Yang, J. Cui, X. Tang, W. Liu, W. Qin, *Dyes and Pigment*, 2013, **98**, 195.

28 N. Agmon, *Chem. Phys. Lett.*, 1995, **244**, 456.

29 M. Eigen, *Angew. Chem. Int. Ed. Engl*, 1964, **3**, 1.

30 (a) T. Kumpulainen, A. M. Brouwer, *Phys. Chem. Chem. Phys*., 2012, **14**, 13019; (b) J. Qian, A. M. Brouwer, *Phys. Chem. Chem. Phys.*, 2010, **12**, 12562.

31 Y. Ooyama, A. Matsugasako, K. Oka, T. Nagano, M. Sumomogi, K. Komaguchi, I. Imae, Y. Harima, *Chem. Commun.*, 2011, **47**, 4448.

32 Y. Ooyama, K. Uenaka, A. Matsugasako, Y. Harima, J. Ohshita, *RSC Adv.,* 2013, **3**, 23255.